

Structural Conservation in Band 4.1, Ezrin, Radixin, Moesin (FERM) Domains as a Guide To Identify Inhibitors of the Proline-Rich Tyrosine Kinase 2

Nathalie Meurice,^{†,‡} Lei Wang,^{‡,‡} Christopher A. Lipinski,^{||} Zhongbo Yang,[⊥] Christopher Hulme,[§] and Joseph C. Loftus^{*,⊥}

[†]The Translational Genomics Research Institute, Phoenix, Arizona 85004, [‡]Tripos International, St. Louis, Missouri 63144, [§]Department of Pharmacology and Toxicology, College of Pharmacy, University of Arizona, Tucson, Arizona 85721, ^{||}Department of Molecular Pharmacology and Experimental Therapeutics, and [⊥]Department of Biochemistry and Molecular Biology, Mayo Clinic Arizona, Scottsdale, Arizona 85239.
[‡]Contributed equally to the manuscript.

Received August 19, 2009

The nonreceptor focal adhesion kinases FAK and Pyk2 play a central role in the regulation of glioma cell proliferation and migration, making them attractive targets to improve clinical outcome. Noncatalytic targeting represents a novel approach to regulate the activity of these tyrosine kinases. A combination of site directed mutagenesis and molecular modeling was used to identify compounds that target the F3 module of the Pyk2 FERM domain. A protein pharmacophore model for the Pyk2 FERM/F3 module, generated utilizing the structural conservation of ligand-bound FERM domains with known 3D structures, was used to search the LeadQuest compound library. Compounds compliant with the model were tested for their ability to inhibit the binding of a monoclonal antibody that maps to a functional site on the F3 module. The highest scoring compound bound directly to the Pyk2 FERM domain, inhibited Pyk2 stimulated glioma migration, and provides the framework for the development of novel therapeutic agents to target the activity of the focal adhesion kinases.

Introduction

Cell–cell adhesion and cell adhesion to specific elements in their surrounding extracellular matrix play a critical role in a number of complex biological processes. The focal adhesion kinase (FAK⁴) and the closely related proline-rich tyrosine kinase 2 (Pyk2) are nonreceptor tyrosine kinases uniquely located to transduce information from interactions with the extracellular matrix and soluble mediators through cell surface integrins, growth factor receptors, and G-protein-coupled receptors to the activation of intracellular signaling pathways that regulate cell migration, proliferation, and survival. By coordinating adhesion and cytoskeletal dynamics with survival and growth signaling, FAK and Pyk2 represent molecular therapeutic targets in cancer cells as malignant cells often exhibit defects in the regulation of these processes. Clinical translation of tyrosine kinase inhibitors has largely focused on competitive inhibition of catalytic domains and has been slowed by the significant conservation of both sequence and structure of these domains. An alternative approach to inhibition of kinase activity is to target protein–protein interactions that play a role in the regulation of kinase activity in order to achieve targeting specificity.^{1,2} Indeed, the past 5 years has witnessed significant progress in the discovery of small molecule inhibitors of protein–protein interactions,^{2–4} and in similar fashion, several new ligands binding

and inhibiting kinase function via an allosteric modality have been reported.^{5–7} On the basis of the success of these studies, we have sought to identify small molecule compounds that target protein–protein interactions that might regulate the kinase activity of Pyk2. The molecules reported herein can be viewed as mechanistic probes and may represent the discovery of a general template that, after further diversification and optimization as has been reported for other protein–protein interaction inhibitors,^{8,9} could lead to new probes for alternative targets of interest in the same family class.

Pyk2 consists of several distinct functional domains including an N-terminal band 4.1, ezrin, radixin, moesin (FERM) domain, a central kinase domain, two C-terminal proline-rich sequences that mediate interactions with proteins containing SH3 domains, and several tyrosine residues that when phosphorylated provide docking sites for SH2 domains.^{10–12} Pyk2 is tyrosine phosphorylated and activated by a variety of stimuli that increase intracellular calcium levels as well as by stress signals. However, it is not well understood how these signals lead to Pyk2 kinase activation. FERM domains are compact clover-shaped structures composed of three structural modules, designated A, B, and C or F1, F2, and F3 respectively, and are typically involved in linking intracellular proteins to the cytoplasmic tails of transmembrane proteins.¹³ Several experimental structures of FERM domains bound to protein fragments from transmembrane protein cytoplasmic tails have been solved by X-ray diffraction (XRD) or nuclear magnetic resonance (NMR).^{14–17} The activity of the classical FERM domain proteins ezrin, radixin, and moesin is known to be regulated by a FERM domain-mediated intramolecular association.^{18–21} Recent studies have demonstrated an autoregulatory function for the FERM domain of FAK.

*To whom correspondence should be addressed. Address: Mayo Clinic Arizona, 13400 E. Shea Boulevard, Scottsdale, AZ 85259. Phone: (480) 301-6274. Fax: (480) 301-8387. E-mail: loftus.joseph@mayo.edu.

^aAbbreviations: FERM, band 4.1, ezrin, radixin, moesin; Pyk2, proline rich tyrosine kinase 2; FAK, focal adhesion kinase; ELISA, enzyme linked immunosorbent assay; LC/MS, liquid chromatography/mass spectrometry.

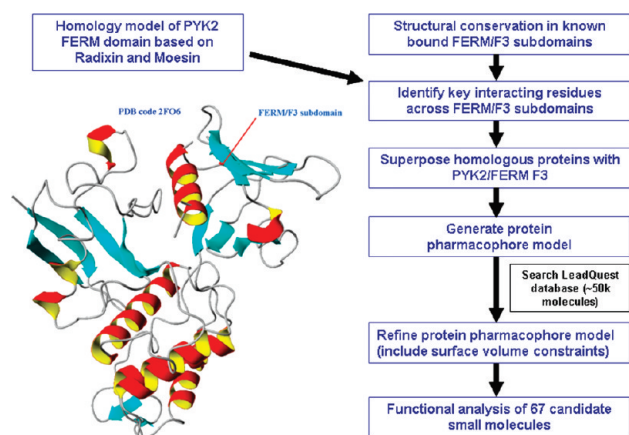


Figure 1. General flowchart describing the in silico search for inhibitors of Pyk2 that interact with the FERM domain at the F3 subdomain by protein pharmacophore-based search of the LeadQuest database.

Structural studies have demonstrated that the FAK FERM domain binds directly to the kinase domain inhibiting access to the catalytic cleft and preventing phosphorylation of the activation loop.²² Although a similar intramolecular interaction between the Pyk2 FERM domain and the Pyk2 kinase domain has not been demonstrated, experimental results nevertheless support a substantive role for the Pyk2 FERM domain in the regulation of Pyk2 activity.^{23–25} Notably, we have demonstrated that selected mutations within the Pyk2 FERM domain inhibited Pyk2 phosphorylation and reduced the capacity of Pyk2 to stimulate glioma cell migration.²⁶ These results suggest that the Pyk2 FERM domain mediates protein–protein interactions that are necessary for Pyk2 function. These observations support the hypothesis that noncatalytic targeting of the Pyk2 FERM domain may provide a novel therapeutic approach to inhibition of Pyk2 activity in tumor cells. In the present study, we utilized structural data of ligand-bound FERM domains and a homology model for Pyk2 FERM (PDB ID 2FO6)²⁶ to define a protein pharmacophore, pinpointing key residues for molecular interaction within the Pyk2 FERM domain. This protein pharmacophore model was then used to search the LeadQuest compound library for compounds likely to compete with protein–protein interactions at the Pyk2 FERM domain. The resulting set of compounds was purchased and assayed, and a lead small molecule was identified that bound to the Pyk2 FERM domain and inhibited Pyk2 function.

Results

General Workflow. The general workflow of the study leading to the identification of compounds inhibiting Pyk2 function at the FERM/F3 subdomain is outlined in Figure 1. This study was accomplished in four major steps: (1) evaluate structural conservation in bound FERM domains with known experimental 3D structures; (2) generate a protein pharmacophore model by similarity of the Pyk2 FERM homology model (PDB ID 2FO6) with other FERM domains in interaction; (3) perform pharmacophore-based search of the LeadQuest database; (4) carry out functional analysis of candidate small molecules.

Structural Conservation in Bound FERM Domains. Previously, we have demonstrated that selected amino acid substitutions within the Pyk2 FERM domain inhibited

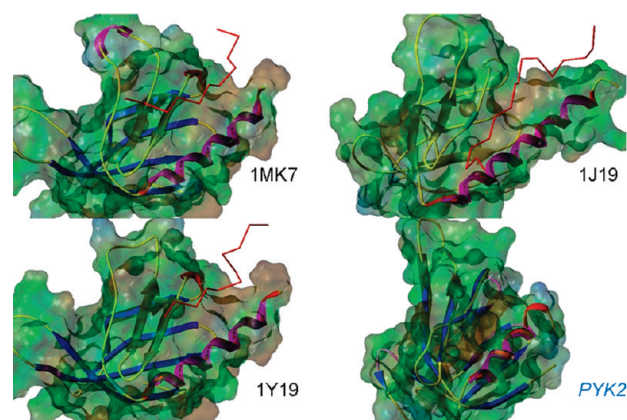


Figure 2. Ribbon representation and overlaid solvent-accessible Connolly surface of ligand-bound talin (PDB IDs 1MK7 and 1Y19), radixin (PDB ID 1J19), and the Pyk2 FERM/F3 homology model. Coloring of solvent-accessible surfaces is based on lipophilic potential. Backbone trace of bound partners is represented as a red wire for the experimental structures (1MK7, 1Y19, and 1J19).

Pyk2 phosphorylation and reduced the capacity of Pyk2 to stimulate glioma migration.²⁶ Furthermore, specific targeting of the $\beta 5C$ - $\alpha 1C$ cleft on the surface of the F3 module of the FERM domain reduced Pyk2 phosphorylation, inhibited glioma migration in vitro, and extended survival in a glioma xenograft model.²⁷ As described in Experimental Procedures, 3D structures of the FERM domains of talin and radixin in interaction with protein fragments were retrieved from the PDB, leading to a set of three homologous protein domains along with their binding partners. An analysis of the structural conservation in these three homologous FERM domains was carried out for the purpose of identifying key residues that are consistently involved in known protein–protein interactions mediated by the cleft between strand $\beta 5C$ and helix $\alpha 1C$ of the F3 lobe. To qualitatively explore the similarity of the physicochemical properties of the $\beta 5C$ - $\alpha 1C$ grooves, solvent accessible surfaces were calculated as described in Experimental Procedures and lipophilic potential was mapped on the surface. The same representation was generated for the FERM/F3 subdomain of Pyk2 homology model for comparison. As illustrated in Figure 2, even though the sequence identities between Pyk2, radixin, and talin are relatively low (<19.5%), their 3D structures present similar topologies and overall shapes. Specifically, the $\beta 5C$ - $\alpha 1C$ grooves that are known to bind protein fragments or peptides present high similarities in terms of their shape and physical properties. Color-coding of solvent-accessible surfaces based on the lipophilic potential reveals conserved hydrophobic patches within the binding sites (Figure 2); the same is true for electrostatic potential mappings as well (Supporting Information Figure 1). These observations reinforced our strategy to utilize structural conservation in the $\beta 5C$ - $\alpha 1C$ grooves of homologous F3 lobes to identify the key residues for protein–protein interactions and then search for equivalent residues in the $\beta 5C$ - $\alpha 1C$ groove of Pyk2.

For a better description of these protein–protein interactions, the $\beta 5C$ - $\alpha 1C$ grooves from the three homologous structures under consideration were examined and hydrogen bonds between the proteins and their relevant binding partners were catalogued (Figure 3a–c). Similar binding patterns were observed: at least three hydrogen bonds were formed between the subdomains and their bound partners in

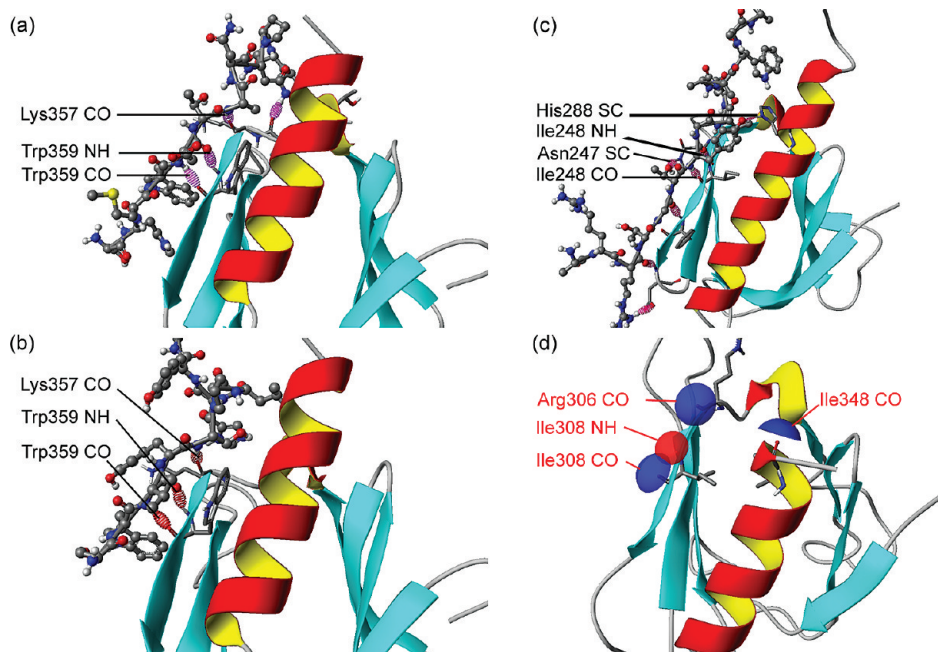


Figure 3. Ribbon representation of FERM/F3 subdomains and conserved specific hydrogen bonds for (a) talin bound with integrin β_3 cytoplasmic domain peptide (1MK7), (b) talin bound with PIP1- γ (1Y19), and (c) radixin bound with ICAM-2 cytoplasmic domain peptide (1J19); (d) mapping of these interactions onto the theoretical structure of the Pyk2 FERM/F3. CO and NH indicate H-bond acceptor and donor atoms on the protein backbones, while SC indicate H-bond interactions with atoms from the protein side chains.

all three crystal structures, anchoring the protein fragments in the binding site. In the case of the bound talin structures (1MK7 and 1Y19), the NH and CO moieties of the backbone of tryptophan 359 are involved in hydrogen bonding with the other protein fragments (Figure 3a and Figure 3b). Similarly in the structure of radixin (1J19), the NH and CO moieties of the backbone of isoleucine 248 also form hydrogen bonds with the ICAM-2 cytoplasmic domain peptide (Figure 3c). This pattern of structural conservation suggests that the capacity of these FERM/F3 residues to form two hydrogen bonds with its binding partner may be important. Additional hydrogen bonds observed in the bound structures involve residues from the β sheets or surrounding loops (talin, 1MK7, and 1Y19) or hydrogen bonding with the side chains of residues located on the α 1C helix (His 288 in radixin complex 1J19, Figure 3c).

Protein Pharmacophore Model. The catalog of interacting residues from the structures of bound FERM domains was utilized to map equivalent residues in the F3 module of the Pyk2 FERM domain and to generate a protein pharmacophore model including both essential and optional constraints. By transposition of the patterns of conserved interactions at the β 5C- α 1C grooves to the 3D theoretical model of Pyk2 (2FO6, Figure 3d), it appeared that Pyk2 FERM F3 residue Ile 308 occupied the structural locus equivalent to Trp 359 in the bound talin structures (1MK7 and 1Y19) and to Ile 248 in the structure of bound radixin (1J19). In addition, the NH and CO moieties of the backbone of Ile 308 are both pointing toward the surface of the groove and hence are available for hydrogen bonding with potential binding partners. Previous mutagenesis data for the Pyk2 FERM domain indicated that substitution of Ile 308 resulted in a loss of Pyk2 activity.²⁶ Other conserved interacting residues catalogued in the β 5C- α 1C grooves of the talin and radixin structures were mapped onto the Pyk2 homology model to pinpoint potential interacting residues of the Pyk2

F3 module. Besides Ile 308, the backbone carbonyl moiety of Arg 306 was identified as equivalent to Lys 357 of talin and subsequently selected as key residue as well. Another interaction with the α 1C helix would be optimal for a small molecule to anchor within the shallow, narrow binding groove, similarly as is observed in the radixin experimental structure (1J19). The CO from the backbone of Ile 348 can serve this purpose, and its importance is confirmed by experimental functional data.²⁷ Together, these results suggest that the β 5C- α 1C groove of Pyk2 FERM domain exhibits properties consistent with protein-protein interaction hot spots.²⁸

In summary, four specific interactions mediated by three residues of Pyk2 FERM/F3 subdomain were selected to form a protein pharmacophore model by similarity with interacting residues in homologous FERM/F3 subdomains with known crystal structures. The four protein pharmacophore features include an H-bond donor/acceptor pair at Ile 308, an H-bond acceptor at Arg 306, and an H-bond acceptor at Ile 348. To build the protein pharmacophore model, the donor/acceptor atoms of each feature were selected and default spatial constraints of 0.5 Å were used to allow some flexibility around the position. The features corresponding to the H-bond donor/acceptor pair at Ile 308 were defined as essential because of the high structural conservation in homologous domains and consistent with the mutagenesis data. As the structures of talin and radixin analyzed above present multiple interactions with the β 5 sheet, the H-bond acceptor feature associated with the Arg 306 CO moiety was also defined as an essential receptor atom. Finally the CO from Ile 348 was defined as an optional constraint, since an equivalent interaction was not observed in all β 5C- α 1C grooves. The final protein pharmacophore model is represented in Figure 4a.

In Silico Identification of Inhibitors of Pyk2 FERM. The protein pharmacophore model was utilized as a query to search the 50K LeadQuest compound library using 3D

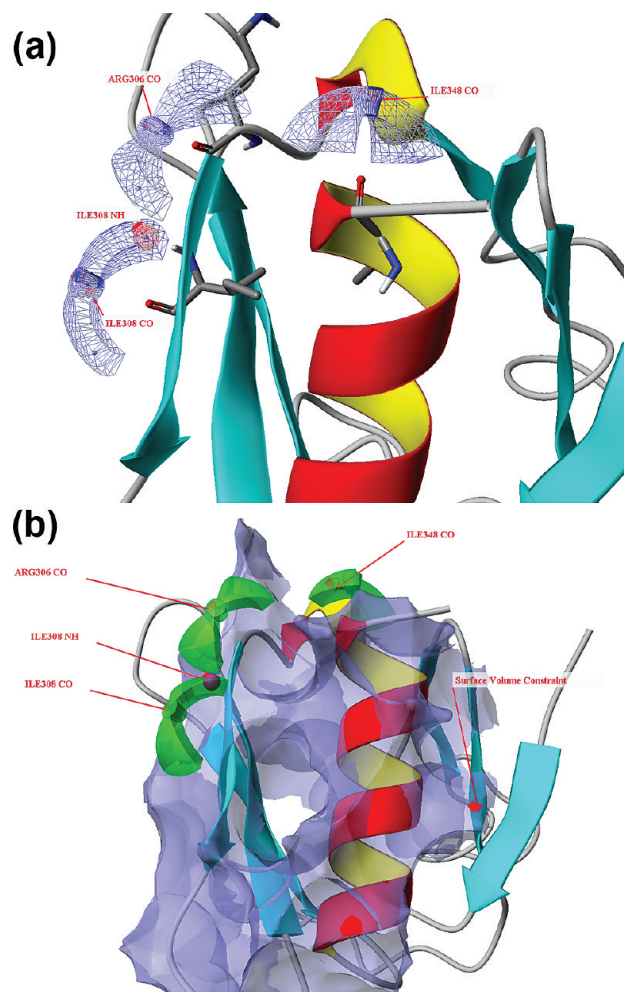


Figure 4. Protein pharmacophore model overlaid on ribbon representation of Pyk2 FERM/F3 subdomain theoretical structure, with labeling of pharmacophore features: (a) initial model with grid representation of spatial constraints and (b) refined model including surface volume constraints in blue and spatial constraints in green.

flexible search (a single conformation of each ligand stored in the database is adjusted to fit the pharmacophore model). Six-hundred-forty-one nonredundant molecules were identified through the initial search process. In order to reduce the number of compounds, the protein pharmacophore model was further refined by adding surface volume constraints for a better definition of the size and shape of the binding groove (Figure 4b). These volume constraints were built using the solvent-accessible surface of the Pyk2 FERM/F3 binding groove and again spatial constraints of 0.5 Å were used to allow some flexibility for steric clashes. By use of the refined protein pharmacophore model, the number of virtual hits was reduced from 641 to 274. Further filtering was carried out on the basis of the Surflex-Dock score of each candidate. Those structures with a Surflex-Dock score greater than 4, which correlates to a K_d of 100 μM , were selected and manually curated. By doing so, 67 compounds with plausible conformation, forming hydrogen bonds in compliance with the protein pharmacophore model, and with minimal steric clash with the binding site were selected, purchased, and evaluated for Pyk2 inhibition in an *in vitro* assay. The 67 selected compounds and their LeadQuest IDs are listed in Supporting Information Figure 2.

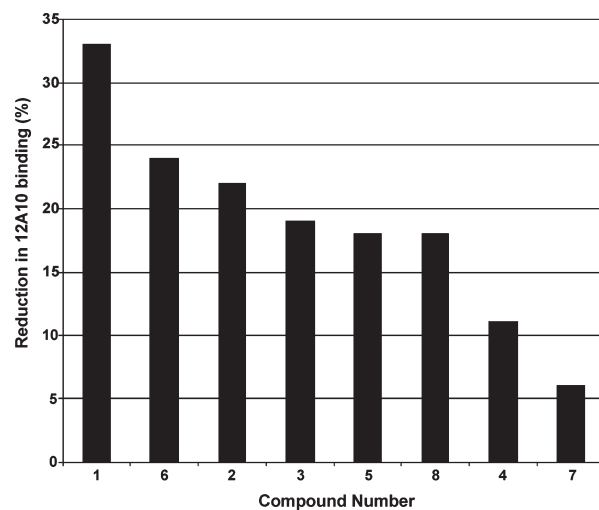


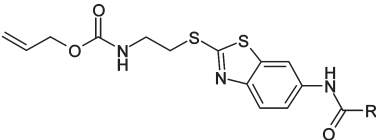
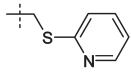
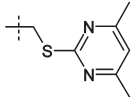
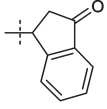
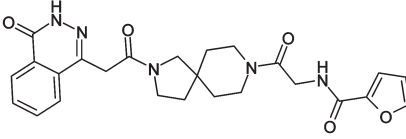
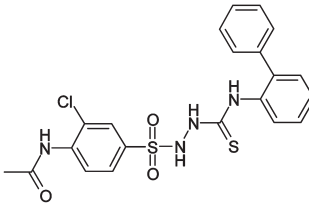
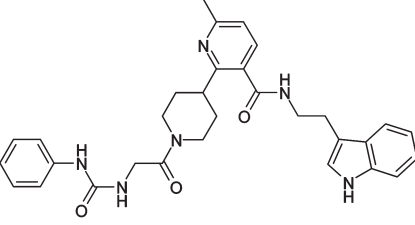
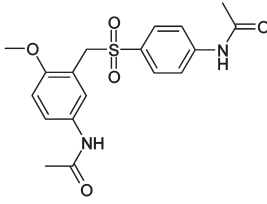
Figure 5. Compound inhibition of antibody 12A10 binding to Pyk2 FERM domain. The binding of the monoclonal antibody 12A10 to the Pyk2 FERM domain in the presence of the specified compounds was assayed by competitive ELISA. Results are presented as reduction of 12A10 binding relative to the binding of 12A10 to the Pyk2 FERM domain in the presence of vehicle alone.

Competitive ELISA Screen. The protein pharmacophore model was built upon a conserved binding site found in other FERM domain-containing proteins. Available ligand-bound FERM domain crystal structures indicated that ligands interacted with a shallow groove on the surface of the FERM/F3 subdomain formed by residues from strand β_5 and helix α_1 . We previously generated a monoclonal antibody, designated 12A10, that reacted specifically with the F3 module of the Pyk2 FERM domain. Site-directed mutagenesis indicated that the epitope of the 12A10 monoclonal antibody mapped to the $\beta_5\text{C}-\alpha_1\text{C}$ surface of the F3 module of the Pyk2 FERM domain.²⁷ Because the epitope of mAb 12A10 mapped to the $\beta_5\text{C}-\alpha_1\text{C}$ surface of the F3 module, we reasoned that mAb 12A10 could be used in a competitive ELISA assay to determine the capacity of the 67 potential compounds to bind to the $\beta_5\text{C}-\alpha_1\text{C}$ surface of the Pyk2 FERM/F3. Successful interaction would be read as inhibition of 12A10 binding. By use of this assay, 8 of the 67 compounds identified in the pharmacophore screen inhibited the binding of 12A10 to purified Pyk2 FERM domain (Figure 5). Inhibition of 12A10 binding ranged between 33% (compound 1) to 6% (compound 7). Activity data for the eight compounds with significant inhibitory behavior is summarized in Table 1. Because compound 1 exhibited the greatest inhibition of 12A10 binding, further analysis was undertaken to examine its interaction with the Pyk2 FERM domain and its effect on glioma migration.

Direct Binding of Compound 1 to Pyk2 FERM. The results of the ELISA suggested that a number of the compounds bound to the Pyk2 FERM domain in an area close to the epitope recognized by the monoclonal antibody 12A10. To validate the direct binding of compound 1 to the Pyk2 FERM domain, we utilized a LC/MS depletion assay. Incubation of compound 1 with purified Pyk2 FERM domain led to a 4-fold reduction in the amount of free compound 1 (Figure 6), indicating a direct uptake of compound 1 by the Pyk2 FERM domain.

Compound 1 Inhibits Glioma Cell *In Vitro* Migration. The capacity of compound 1 to inhibit the binding of the site specific antibody 12A10 suggested that an interaction was

Table 1. Compound Labeling, LeadQuest ID, Activity, and 2D Structures of Eight Confirmed Actives^a

ID	LeadQuest ID	Inhibition of 12A10 binding (%)	2D structure	
			Scaffold	R
1	1542-03639	33		
2	1542-03119	22		
3	1542-03084	19		
4	1542-03102	11		
5	1520-00790	18		
6	1538-01282	24		
7	1548-00166	6		
8	1554-01507	18		

^a Activity is expressed as the percentage of inhibition of 12A10 binding as assayed by competitive ELISA.

occurring between this candidate small molecule and the Pyk2 FERM domain. The LC/MS depletion assay substantiated a direct interaction of compound **1** with the Pyk2 FERM domain. However, neither of these assays can accurately predict whether compound **1** can interact with and functionally inhibit endogenous intracellular Pyk2. We have

previously demonstrated that knockdown of Pyk2 expression or inhibition of Pyk2 activity significantly inhibited glioma cell migration and prolongs survival in orthotopic xenograft mouse disease models.^{29,30} Therefore, we examined the capacity of compound **1** to inhibit the Pyk2-mediated stimulation of glioma cell migration. The migration rate of SF767 glioma

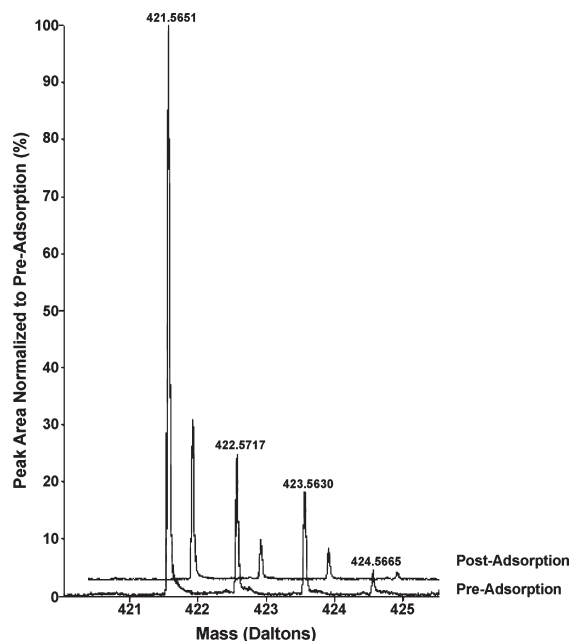


Figure 6. Binding of compound **1** to purified Pyk2 FERM domain. A solution of compound **1** (1 mg/mL) without addition of purified Pyk2 FERM domain (preadsorption) or after addition of purified Pyk2 FERM domain was incubated for 1 h at 37 °C and then analyzed by LC/MS. The decrease in free compound **1** after addition of Pyk-FERM shows the direct uptake of compound **1**.

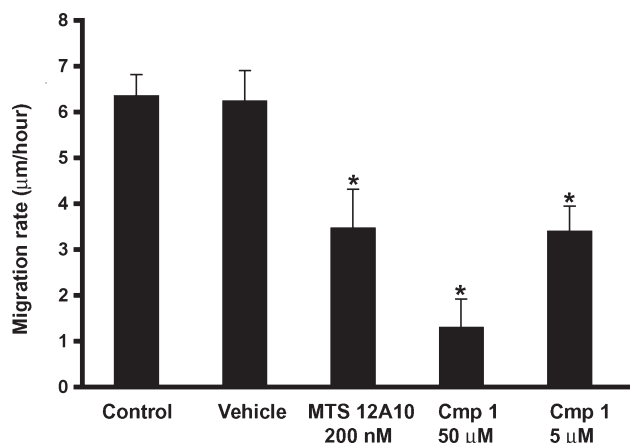


Figure 7. Compound **1** inhibits glioma cell migration. SF767 glioma cells were left untreated (control), treated with vehicle alone, or treated with compound **1** or MTS-12A10 antibody at the indicated concentrations for 16 h and plated on laminin, and the migration rates were determined by radial migration assay: (*) $p < 0.05$.

cells cultured in the presence of 5 μM compound **1** was reduced nearly 50% relative to vehicle treated cells (Figure 7). This compared favorably to treatment of SF767 cells with monoclonal antibody 12A10 chemically conjugated to membrane transport sequence peptides³¹ that inhibited migration ~50% at 200 nM.²⁷ Treatment of SF767 cells with compound **1** at 50 μM inhibited migration by 85%.

Discussion

We have previously reported that the N-terminal FERM domain of Pyk2 plays a central role in the regulation of Pyk2 activity. In the current study, we investigated the functional potential of targeting the F3 subdomain of the Pyk2 FERM as a means to regulate the activity of Pyk2. The major findings of

this report are as follows: (1) a protein pharmacophore model for the Pyk2 FERM domain F3 module was generated utilizing the structural conservation of bound FERM domains with known 3D structures; (2) a pharmacophore-based search of the LeadQuest database identified 67 compounds compliant with the model; (3) 8 of the identified 67 compounds inhibited the binding of a monoclonal antibody specific for the F3 module; (4) the compound with the greatest inhibition of antibody binding bound directly to the Pyk2 FERM domain and inhibited the Pyk2 stimulated glioma cell migration. Together these data validate the approach of combining experimental mutagenesis and computational methodologies to identify small molecule ligands for the Pyk2 FERM domain that inhibit Pyk2 function.

The FERM domain is a conserved protein module that mediates both protein–membrane targeting and protein–protein interactions. Protein–membrane targeting is mediated by basic residues in a cleft between subdomains F1 and F3 that interact with PIP2.^{16,32} Interaction of FERM domains with PIP2 molecules at the membrane has been proposed to induce conformational changes that unmask the full-length FERM proteins and stimulate their interaction with the cytoplasmic tails of transmembrane proteins.³³ High resolution structures for ligand bound FERM domains indicate that these interactions are mediated by residues in the F3 subdomain.^{14,15,17,33} The F3 subdomain exhibits a fold typical of a phosphotyrosine-binding (PTB) or pleckstrin homology (PH) domain consisting of a seven-stranded β sandwich followed by a long α helix at the C-terminus. The binding interactions occur in a long shallow groove on the surface of F3 formed by residues from $\beta 5\text{C}$ and $\alpha 1\text{C}$. Although the Pyk2 FERM domain lacks the PIP2 binding site observed in classical ERM proteins, the amino acids in the $\beta 5\text{C}$ - $\alpha 1\text{C}$ groove that mediate peptide recognition are conserved in the Pyk2 F3 subdomain. Notably, Pyk2 I308 in $\beta 5\text{C}$ is highly conserved among FERM domains and substitution of this residue significantly inhibited Pyk2 phosphorylation.²⁶ This suggests that the $\beta 5\text{C}$ - $\alpha 1\text{C}$ surface of the Pyk2 FERM domain may be critical for an interaction that plays a role in the regulation of its activity. Thus, existing structural data for related FERM domains could provide the framework for the identification of inhibitors targeting this site.

Available 3D experimental structures of related bound FERM domains were thus used to provide insights into conserved amino acids playing key roles in protein–protein interactions at the $\beta 5\text{C}$ - $\alpha 1\text{C}$ groove. Comparison of the binding mode of radixin-ICAM2 (1J19), talin- $\beta 3$ integrin cytoplasmic tail (1MK7), and talin-PIP2 type 1 γ (1Y19) demonstrated that a conserved binding pattern was utilized in each case. Specifically, in all three crystal structures at least three hydrogen bonds were formed between the F3 subdomain and their bound partners anchoring the protein fragments in the binding site.

The structural features of our Pyk2 FERM domain 3D homology model (2FO6) are revealing. In particular, amino acid residues in the $\beta 5\text{C}$ - $\alpha 1\text{C}$ groove that mediate peptide recognition for other FERM domains are conserved when mapped onto the F3 module of the Pyk2 FERM subdomain. When transferred to the Pyk2 FERM F3 module, these highly conserved features include moieties of the residues Ile 308, Arg 306, and Ile 348. The H-bond donor/acceptor features of these three residues were assembled into a protein pharmacophore model capturing the conservation of the homologous bound FERM domains mapped onto Pyk2 FERM. Four features

were defined, namely, an H-bond donor/acceptor pair at Ile 308, an H-bond acceptor at Arg 306, an H-bond acceptor at Ile 348, and spatial constraints and volume restraints. Note that these three residues present typical profiles of “hot spot” residues for protein–protein interaction interfaces.³⁴ Indeed, these hotspots are typically made up of a small subset of residues at the interface enriched in tryptophan, tyrosine, and arginine residues. Isoleucine, aspartic acid, and histidine also show enrichment in hot spots. These results suggest that the three selected residues, accounting for four specific interactions in the protein pharmacophore, are certainly relevant to protein–protein interactions. They also support our hypothesis that a perspective small molecule ligand is not required to cover the entire binding interface to perturb the interaction, but rather it may perturb the interaction by interacting specifically with the hot spot residues.

Following this logic, the protein pharmacophore established on the basis of the structural conservation in protein families was utilized to interrogate the LeadQuest database (50K compounds) for the purpose of identifying compounds candidates fitting the 3D pharmacophore model, following a multistep process. The query included a flexible search that identified 641 molecules at first hand. Next, volume constraints were added reducing the number of hits to 274. Further curation was carried out on the basis of scoring and other criteria including plausibility of conformations, leading to the final set of 67 compounds selected for assay. These 67 molecules cover 10 different chemotype classes presented in Supporting Information. Chemotypes with identifiers 1542, 1506, and 1548 present the highest compound density and are populated by, respectively, 24, 18, and 8 compounds. Three classes with identifiers 1518, 1520, and 1533 are populated by 4 compounds. The chemotypic class 1538 includes 2 molecules, and all other chemotypes are singletons. Eight of these compounds presented significant activity in the 12A10 antibody binding competition assay, and these 8 actives populate 5 different chemotype classes with identifiers 1520 (1 active), 1538 (1 active), 1542 (4 actives), 1548 (1 active), and 1554 (1 active). It clearly appears that a reinforced activity signal is observed for the benzothiazole chemotype 1542. All other classes are isolated actives and would require further structure–activity relationships investigation to ascertain the value of such chemotypes as screening hits.

Previously, we generated the monoclonal antibody 12A10 that recognizes an epitope located on the $\beta 5C$ - $\alpha 1C$ surface of the F3 module and overlaps a site that plays a role in Pyk2 activity.²⁷ Conjugation of the 12A10 antibody to a membrane transport peptide that facilitated intracellular accumulation or stable intracellular expression of a single chain Fv fragment of 12A10 inhibited glioma cell migration supporting a functional role for this site in the regulation of Pyk2 activity. Several compounds identified in the virtual screen inhibited the binding of 12A10, suggesting that they bound to a site that overlaps with the 12A10 epitope. Indeed, compound **1** was shown to bind directly to the Pyk2 FERM domain and inhibited Pyk2 stimulated glioma migration. These results suggest that compound **1** was potentially mimicking the inhibitory activity of 12A10 by interacting with a site that overlaps with the 12A10 binding site. The molecular basis for this inhibition remains to be determined but may result from the ability of 12A10 or compound **1** to block the proposed FERM mediated formation of a Pyk2 homodimer.²⁵ Alternatively, compound **1** could competitively inhibit FERM/F3 mediated protein–protein interactions that regulate Pyk2

activity. This later possibility is supported by the demonstration that the $\beta 5C$ - $\alpha 1C$ surface of the F3 module of homologous FERM domains serves as the recognition site for a number of ligands.^{14,15,33,35–37} The identity of proteins that interact with this site in the Pyk2 FERM domain is an area of ongoing investigation.

In summary, we utilized the structural conservation of three homologous FERM domains to identify key residues that are consistently involved in known protein–protein interactions mediated by the cleft between strand $\beta 5C$ and helix $\alpha 1C$ of the F3 subdomain. The catalog of interacting residues from the structures of bound FERM domains was utilized to map equivalent residues in the F3 module of the Pyk2 FERM domain and to generate a protein pharmacophore model. The model was used to virtually search for compounds that would target this site in the Pyk2 FERM domain. Eight of the compounds identified as potential ligands for this site inhibited the binding of a monoclonal antibody that maps to this site. Because the compound with the greatest inhibition of antibody binding bound directly to the Pyk2 FERM domain and inhibited the Pyk2 stimulated glioma cell migration, the compounds identified in this study serve as leads for the development of novel therapeutic agents to target the activity of the focal adhesion kinase Pyk2 in glioma. Further, since Pyk2 plays a critical role in the migration of osteoclasts and immune cells, such molecules may possess therapeutic potential in inflammation and osteoporotic disease.

Experimental Procedures

3D Structures of FERM Domains. Chain B from the crystal structure of an integrin β_3 -talin chimera (PDB code 1MK7),¹⁵ along with the crystal structure of the radixin FERM bound to the ICAM-2 cytoplasmic domain peptide (PDB code 1J19),³³ and chain D from the crystal structure of the talin FERM bound to phosphatidylinositol phosphate kinase type I- γ ¹⁴ (PDB code 1Y19) were used as the basis to study the structural basis for the interaction between FERM F3 domains and protein fragment ligands.

Molecular Modeling. Molecular modeling studies were carried out using the SYBYL suite of software (SYBYL Molecular Modeling System, version 7.3, Tripos International, St. Louis, MO) with different add-on modules (biopolymer, MOLCAD, CONCORD, Unity, Surflex-Dock) on a IBM PC with Pentium M processor, 2 GHz CPU, and 2 GB of RAM running Redhat Linux Enterprise 4.0.

MOLCAD was used to create graphical images, to compute and visualize molecular surfaces of the proteins under consideration, and to map three-dimensional (3D) physicochemical properties onto the surfaces.³⁸ Specifically in this study, lipophilic potential and cavity depths were displayed on fast Connolly solvent-accessible surfaces for qualitative analysis of surface similarity between binding grooves of available experimental 3D structures and the PYK2 homology model. All default parameters were used. The Biopolymer module was used to prepare protein structures from the crystal structures cited above by retaining only the F3 FERM subdomain and by adding hydrogens.

The key residues from the FERM F3 subdomains that interact through hydrogen bonds with protein fragments or peptides under consideration were identified from the crystal structures and used to align the structures together. Least squares fitting was performed by using the backbone atoms from the key residues. Residues capable of forming equivalent interactions in Pyk2 were pinpointed and aligned with the other structures under consideration using the Biopolymer module. Protein donor atom and acceptor atoms from the residues on the surface were selected, and spatial constraints were built by using Unity; a default 0.5 Å radius was used for all the constraints in Unity.

Surface volume constraints were created by calculating a MOLCAD surface for the binding sites and then by expanding the surface uniformly outward with 1.0 Å tolerance, 0.5 Å overlap, and 1 Å van der Waals scaling.

Search for Pyk2 FERM Inhibitors in LeadQuest. Tripos LeadQuest database was used as the chemical space for this study. Specifically, the April 2006 version of Leadquest containing 51 068 compounds was prefiltered with Lipinski flags and queried using the 3D pharmacophore search protocol implemented in Unity flexible search, with all options set as default (UNITY Chemical Information Software, version 7.3; Tripos Inc., St. Louis, MO). In the Unity search protocol, the conformations of the compound database were generated on the fly by means of the Directed Tweak method implemented in CONCORD.³⁸ The maximum time per structure, which affects the thoroughness of the conformational search, was set to 60s. Given that LeadQuest includes only druglike compounds and that prefiltering was carried out as a preliminary step, Lipinski's rule of 5 filters were turned off during the search. Compounds were ranked on the basis of the Surfex-Dock scoring scheme, relying on a Protomol-based representation of putative ligands and employing an empirically derived function including hydrophobic, polar, repulsive, entropic, and solvation terms that estimate dissociation constants (K_d) expressed in $-\log(K_d)$ unit.^{39–41} Pre- and postminimization along with a search for low-energy ring conformations were carried out, and default values were used for all other parameters. A cutoff score of 4 from Surfex-Dock, which corresponds to a K_d of 100 μM ,⁴¹ combined with visual inspection was used for final filtering of the hit compounds from the database search.

Generation of 12A10 Antibody. The generation and characterization of the monoclonal antibody 12A10 have been previously described.²⁷ Briefly, recombinant 6X His epitope-tagged Pyk2 F3 protein encoding amino acid residues D261–A366 was produced in *E. coli* strain BL21. Protein expression was induced by the addition of IPTG (isopropyl β -D-thiogalactopyranoside) to a final concentration of 0.1 mM. Induced cultures were grown for 60 min at 30 °C, and bacterial cells were pelleted and frozen at –80 °C. Bacterial cell lysates were clarified by centrifugation, and recombinant F3 was purified by batch adsorption on a Ni-NTA resin followed by FPLC on a Resource Q column (GE Healthcare). Monoclonal antibodies were raised against purified F3 immunogen using standard techniques. The 12A10 hybridoma is isotype IgG₁.

Competition ELISA. Compounds selected by structure-based pharmacophore search in the LeadQuest compound database were purchased from Tripos Inc. Each compound was soluble in PBS containing 1% DMSO. The purity reported by the manufacturer was greater than 95% and was checked by testing three random compounds by LC/MS and verified. To screen each compound, the HA epitope-tagged Pyk2 FERM domain expressed in 293 cells was captured in an Immulon II 96-well plate by adding 100 μg of cell lysate to wells coated with rabbit anti-HA monoclonal antibody. After capture, wells were washed 3 \times with PBS containing 0.2% Tween-20. Unbound sites were blocked by addition of 200 μL of SuperBlock blocking solution (Pierce Biochemical) containing 0.05% Tween-20 (SBBST) for 1 h at room temperature. Compounds from a 10 mM stock solution in DMSO were diluted in SBBST to a final concentration of 400 μM and then added to the wells for 1 h followed by addition of 110 nM of the 12A10 antibody in an equal volume of SBBST. Following incubation for an additional hour at room temperature, wells were washed 3 \times with PBS containing 0.2% Tween-20 and bound 12A10 antibody was detected by incubation with an HRP-conjugated goat-antimouse (Fc γ fragment specific) antibody. The total absorbance (OD₄₉₀) from the colorimetric assay for each compound was compared to the control signal of the binding of 12A10 to Pyk2 FERM in vehicle only (5% DMSO final in SBBST) to calculate the percentage of binding inhibition. Preliminary experiments indicated that the

binding of 12A10 to captured Pyk2 FERM was not affected by DMSO concentrations up to 20%. The data represent that observed for at least six replicate assays. Within-group variance was determined by ANOVA and the between-group mean comparisons were assessed by Mann–Witney *U* significance testing. Statistical reduction in 12A10 binding was defined at a significance level of $p < 0.05$.

LCMS Depletion Assay. Compound **1** (2.37 mM) alone or compound **1** (2.37 mM) together with HPLC purified recombinant Pyk2 FERM domain (0.5 mM) was incubated at 37 °C for 1 h, after which the sample was analyzed by LC/MS. Samples were diluted in buffer (25 mM ammonium bicarbonate, 5% acetonitrile, and 0.1% formic acid) and placed into a sample manager of a Waters Acquity ultrahigh performance liquid chromatograph (UPLC) at 4 °C. An amount of 5 μL of sample was injected onto an Acquity C18 1.7 μm , 2.1 mm \times 50 mm liquid chromatography column (all runs performed in triplicate) and run for a total of 12 min in a 5–100% water to acetonitrile gradient using a 0.1% formic acid additive. LC/MS configuration for these experiments was as follows: (1) operating mode set to ESI positive ion, (2) internal optics set in the W configuration, (3) capillary voltage was constant at 3.2 kV, (4) sample cone voltage was at 100 V, and (5) desolvation gas flow of 700 L/h and cone gas flow of 20 L/h. The column retention time and mass spectrogram were determined for free compound **1** injected alone or in the presence of HPLC purified recombinant Pyk2 FERM domain to determine the depletion of free compound **1**.

Cell Migration Assay. To determine whether blocking of a site-specific monoclonal antibody had any correlation to modulation of a relevant cellular phenotype, the compound with greatest inhibitory activity in competitive ELISA (compound **1**) was evaluated for the capacity to inhibit in vitro migration. The radial migration assay has been previously described in detail.⁴² Briefly, glass slides containing 10 individual 7 mm circular seeding areas surrounded by a hydrophobic template mask were coated with laminin (10 $\mu\text{g}/\text{mL}$). Control or treated cells were resuspended in DMEM containing 10% serum with or without treatment agent and seeded at a density of 2500 cells per well of a cell sedimentation manifold (Creative Scientific Methods Inc., Phoenix, AZ). After overnight incubation (16 h), the manifold was removed and an initial measurement (t_0) of the diameter of the cell colony was made using an inverted microscope and image analysis software (Scion Image, Frederick, MD). The change in the diameter of the cell population over time was determined at 24 h following the initial measurement. Slopes of the lines derived from the measurements (radius versus time) were used to calculate the migration rate of the cells. Linear migration from the initial seeded area at t_0 was determined for at least 10 replicate samples for each treatment. Specific migration rates were calculated by normalizing the measurements to nonspecific migration on BSA. The absolute migration and migratory rates were calculated and group mean values determined.

Acknowledgment. We thank Dr. Nhan Tran and Matthew Ennis for their assistance with the cell migration assay. This work was supported by grants from the National Institutes of Health (Grants CA 103956 and CA 108961 to J.C.L.).

Supporting Information Available: Electrostatic potential mappings and chemotypes of selected compounds. This material is available free of charge via the Internet at <http://pubs.acs.org>.

References

- (1) Sperandio, O.; Miteva, M.; Segers, K.; Nicolaes, G. A. F.; Villoutreix, B. O. Screening outside the catalytic site: inhibition of macromolecular interactions through structure-based virtual ligand screening experiments. *Open Biochem. J.* **2008**, *2*, 29–37.

- (2) Wells, J. A.; McClendon, C. L. Reaching for high-hanging fruit in drug discovery at protein–protein interfaces. *Nature* **2007**, *450*, 1001–1009.
- (3) Domling, A. Small molecular weight protein–protein interaction antagonists—an insurmountable challenge? *Curr. Opin. Chem. Biol.* **2008**, *12*, 281–291.
- (4) Ruffner, H.; Bauer, A.; Bouwmeester, T. Human protein–protein interaction networks and the value for drug discovery. *Drug Discovery Today* **2007**, *12*, 709–716.
- (5) Lewis, J. A.; Lebois, E. P.; Lindsley, C. W. Allosteric modulation of kinases and GPCRs: design principles and structural diversity. *Curr. Opin. Chem. Biol.* **2008**, *12*, 269–280.
- (6) Liu, Y.; Gray, N. S. Rational design of inhibitors that bind to inactive kinase conformations. *Nat. Chem. Biol.* **2006**, *2*, 358–364.
- (7) Zhao, Z.; Robinson, R. G.; Barnett, S. F.; Defeo-Jones, D.; Jones, R. E.; Hartman, G. D.; Huber, H. E.; Duggan, M. E.; Lindsley, C. W. Development of potent, allosteric dual Akt1 and Akt2 inhibitors with improved physical properties and cell activity. *Bioorg. Med. Chem. Lett.* **2008**, *18*, 49–53.
- (8) Parks, D. J.; LaFrance, L. V.; Calvo, R. R.; Milkiewicz, K. L.; Gupta, V.; Lattanze, J.; Ramachandren, K.; Carver, T. E.; Petrella, E. C.; Cummings, M. D.; Maguire, D.; Grasberger, B. L.; Lu, T. 1,4-Benzodiazepine-2,5-diones as small molecule antagonists of the HDM2-p53 interaction: discovery and SAR. *Bioorg. Med. Chem. Lett.* **2005**, *15*, 765–770.
- (9) Parks, D. J.; LaFrance, L. V.; Calvo, R. R.; Milkiewicz, K. L.; Marugan, J.; Raboisson, P.; Schubert, C.; Koblisch, H. K.; Zhao, S.; Franks, C. F.; Lattanze, J.; Carver, T. E.; Cummings, M. D.; Maguire, D.; Grasberger, B. L.; Maroney, A. C.; Lu, T. Enhanced pharmacokinetic properties of 1,4-benzodiazepine-2,5-dione antagonists of the HDM2-p53 protein–protein interaction through structure-based drug design. *Bioorg. Med. Chem. Lett.* **2006**, *16*, 3310–3314.
- (10) Avraham, S.; London, R.; Fu, Y.; Ota, S.; Hiregowdara, D.; Li, J.; Jiang, S.; Pasztor, L. M.; White, R. A.; Groopman, J. E.; et al. Identification and characterization of a novel related adhesion focal tyrosine kinase (RAFTK) from megakaryocytes and brain. *J. Biol. Chem.* **1995**, *270*, 27742–27751.
- (11) Lev, S.; Moreno, H.; Martinez, R.; Canoll, P.; Peles, E.; Musacchio, J. M.; Plowman, G. D.; Rudy, B.; Schlessinger, J. Protein tyrosine kinase PYK2 involved in Ca^{2+} -induced regulation of ion channel and MAP kinase functions. *Nature* **1995**, *376*, 737–745.
- (12) Sasaki, H.; Nagura, K.; Ishino, M.; Tobioka, H.; Kotani, K.; Sasaki, T. Cloning and characterization of cell adhesion kinase beta, a novel protein–tyrosine kinase of the focal adhesion kinase subfamily. *J. Biol. Chem.* **1995**, *270*, 21206–21219.
- (13) Mangeat, P.; Roy, C.; Martin, M. ERM proteins in cell adhesion and membrane dynamics. *Trends Cell Biol.* **1999**, *9*, 187–192.
- (14) de Pereda, J. M.; Wegener, K. L.; Santelli, E.; Bate, N.; Ginsberg, M. H.; Critchley, D. R.; Campbell, I. D.; Liddington, R. C. Structural basis for phosphatidylinositol phosphate kinase type I- γ binding to talin at focal adhesions. *J. Biol. Chem.* **2005**, *280*, 8381–8386.
- (15) Garcia-Alvarez, B.; de Pereda, J. M.; Calderwood, D. A.; Ulmer, T. S.; Critchley, D.; Campbell, I. D.; Ginsberg, M. H.; Liddington, R. C. Structural determinants of integrin recognition by talin. *Mol. Cell* **2003**, *11*, 49–58.
- (16) Hamada, K.; Shimizu, T.; Matsui, T.; Tsukita, S.; Hakoshima, T. Structural basis of the membrane-targeting and unmasking mechanisms of the radixin FERM domain. *EMBO J.* **2000**, *19*, 4449–4462.
- (17) Wegener, K. L.; Partridge, A. W.; Han, J.; Pickford, A. R.; Liddington, R. C.; Ginsberg, M. H.; Campbell, I. D. Structural basis of integrin activation by talin. *Cell* **2007**, *128*, 171–182.
- (18) Edwards, S. D.; Keep, N. H. The 2.7 Å crystal structure of the activated FERM domain of moesin: an analysis of structural changes on activation. *Biochemistry* **2001**, *40*, 7061–7068.
- (19) Li, Q.; Nance, M. R.; Kulikauskas, R.; Nyberg, K.; Fehon, R.; Karplus, P. A.; Bretscher, A.; Tesmer, J. J. Self-masking in an intact ERM–merlin protein: an active role for the central alpha-helical domain. *J. Mol. Biol.* **2007**, *365*, 1446–1459.
- (20) Pearson, M. A.; Reczek, D.; Bretscher, A.; Karplus, P. A. Structure of the ERM protein moesin reveals the FERM domain fold masked by an extended actin binding tail domain. *Cell* **2000**, *101*, 259–270.
- (21) Smith, W. J.; Nassar, N.; Bretscher, A.; Cerione, R. A.; Karplus, P. A. Structure of the active N-terminal domain of ezrin. Conformational and mobility changes identify keystone interactions. *J. Biol. Chem.* **2003**, *278*, 4949–4956.
- (22) Lietha, D.; Cai, X.; Ceccarelli, D. F.; Li, Y.; Schaller, M. D.; Eck, M. J. Structural basis for the autoinhibition of focal adhesion kinase. *Cell* **2007**, *129*, 1177–1187.
- (23) Dunty, J. M.; Gabarra-Niecko, V.; King, M. L.; Ceccarelli, D. F.; Eck, M. J.; Schaller, M. D. FERM domain interaction promotes FAK signaling. *Mol. Cell. Biol.* **2004**, *24*, 5353–5368.
- (24) Dunty, J. M.; Schaller, M. D. The N termini of focal adhesion kinase family members regulate substrate phosphorylation, localization, and cell morphology. *J. Biol. Chem.* **2002**, *277*, 45644–45654.
- (25) Kohno, T.; Matsuda, E.; Sasaki, H.; Sasaki, T. Protein–tyrosine kinase $CAK\beta$ /PYK2 is activated by binding Ca^{2+} /calmodulin to FERM F2 $\alpha 2$ helix and thus forming its dimer. *Biochem. J.* **2008**, *410*, 513–523.
- (26) Lipinski, C. A.; Tran, N. L.; Dooley, A.; Pang, Y. P.; Rohl, C.; Kloss, J.; Yang, Z.; McDonough, W.; Craig, D.; Berens, M. E.; Loftus, J. C. Critical role of the FERM domain in Pyk2 stimulated glioma cell migration. *Biochem. Biophys. Res. Commun.* **2006**, *349*, 939–947.
- (27) Loftus, J. C.; Yang, Z.; Tran, N. L.; Kloss, J.; Viso, C.; Berens, M. E.; Lipinski, C. A. The Pyk2 FERM domain as a target to inhibit glioma migration. *Mol. Cancer Ther.* **2009**, *8*, 1505–1514.
- (28) Moreira, I. S.; Fernandes, P. A.; Ramos, M. J. Hot spots. A review of the protein–protein interface determinant amino-acid residues. *Proteins* **2007**, *68*, 803–812.
- (29) Lipinski, C. A.; Tran, N. L.; Menashi, E.; Rohl, C.; Kloss, J.; Bay, R. C.; Berens, M. E.; Loftus, J. C. The tyrosine kinase pyk2 promotes migration and invasion of glioma cells. *Neoplasia* **2005**, *7*, 435–445.
- (30) Lipinski, C. A.; Tran, N. L.; Viso, C.; Kloss, J.; Yang, Z.; Berens, M. E.; Loftus, J. C. Extended survival of Pyk2 or FAK deficient orthotopic glioma xenografts. *J. Neuro-Oncol.* **2008**, *90*, 181–189.
- (31) Zhao, Y.; Lou, D.; Burkett, J.; Kohler, H. Chemical engineering of cell penetrating antibodies. *J. Immunol. Methods* **2001**, *254*, 137–145.
- (32) Hirao, M.; Sato, N.; Kondo, T.; Yonemura, S.; Monden, M.; Sasaki, T.; Takai, Y.; Tsukita, S. Regulation mechanism of ERM (ezrin/radixin/moesin) protein/plasma membrane association: possible involvement of phosphatidylinositol turnover and Rho-dependent signaling pathway. *J. Cell Biol.* **1996**, *135*, 37–51.
- (33) Hamada, K.; Shimizu, T.; Yonemura, S.; Tsukita, S.; Hakoshima, T. Structural basis of adhesion-molecule recognition by ERM proteins revealed by the crystal structure of the radixin-ICAM-2 complex. *EMBO J.* **2003**, *22*, 502–514.
- (34) Bogan, A. A.; Thorn, K. S. Anatomy of hot spots in protein interfaces. *J. Mol. Biol.* **1998**, *280*, 1–9.
- (35) Eck, M. J.; Dhe-Paganon, S.; Trub, T.; Nolte, R. T.; Shoelson, S. E. Structure of the IRS-1 PTB domain bound to the juxtamembrane region of the insulin receptor. *Cell* **1996**, *85*, 695–705.
- (36) Li, S.-C.; Zwahlen, C.; Vincent, S. J. F.; McGlade, C. J.; Kay, L. E.; Pawson, T.; Forman-Kay, J. D. Structure of a Numb PTB domain–peptide complex suggests a basis for diverse binding specificity. *Nat. Struct. Mol. Biol.* **1998**, *5*, 1075–1083.
- (37) Zhang, Z.; Lee, C.-H.; Mandiyan, V.; Borg, J.-P.; Margolis, B.; Schlessinger, J.; Kuriyan, J. Sequence-specific recognition of the internalization motif of the Alzheimer’s amyloid precursor protein by the X11 PTB domain. *EMBO J.* **1997**, *16*, 6141–6150.
- (38) Keil, M.; Exner, T. E.; Brickmann, J. Pattern recognition strategies for molecular surfaces: III. Binding site prediction with a neural network. *J. Comput. Chem.* **2004**, *25*, 779–789.
- (39) Jain, A. N. Surfex: fully automatic flexible molecular docking using a molecular similarity-based search engine. *J. Med. Chem.* **2003**, *46*, 499–511.
- (40) Jain, A. N. Virtual screening in lead discovery and optimization. *Curr. Opin. Drug Discovery Dev.* **2004**, *7*, 396–403.
- (41) Pham, T. A.; Jain, A. N. Parameter estimation for scoring protein–ligand interactions using negative training data. *J. Med. Chem.* **2006**, *49*, 5856–5868.
- (42) Lipinski, C. A.; Tran, N. L.; Bay, C.; Kloss, J.; McDonough, W. S.; Beaudry, C.; Berens, M. E.; Loftus, J. C. Differential role of proline-rich tyrosine kinase 2 and focal adhesion kinase in determining glioblastoma migration and proliferation. *Mol. Cancer Res.* **2003**, *1*, 323–332.